Realistic master equation modeling of relaxation on complete potential energy surfaces: Partition function models and equilibrium results

Keith D. Ball and R. Stephen Berry

Citation: The Journal of Chemical Physics **109**, 8541 (1998); doi: 10.1063/1.477520
View online: http://dx.doi.org/10.1063/1.477520
View Table of Contents: http://scitation.aip.org/content/aip/journal/jcp/109/19?ver=pdfcov
Published by the AIP Publishing

Realistic master equation modeling of relaxation on complete potential energy surfaces: Partition function models and equilibrium results

Keith D. Ball
Department of Physics and The James Franck Institute, The University of Chicago, Chicago, Illinois 60637

R. Stephen Berry
Department of Chemistry and The James Franck Institute, The University of Chicago, Chicago, Illinois 60637

(Received 6 May 1998; accepted 14 August 1998)

To elucidate the role that potential surface topography plays in shaping the evolution of a cluster toward equilibrium, entire sets of kinetically accessible bound-state configurations and transition states on the model potential energy surfaces of $(KCl)_5$ and Ar_9 are mapped and compared. To describe the stochastic dynamics on these surfaces in terms of transition-state theory, we require adequate approximations of the partition functions of the minima and transition states. In this paper we introduce several partition function models derived from harmonic and anharmonic approximations and compare their predicted equilibrium population distributions with those determined from canonical-ensemble molecular dynamics. We perform this comparison for both $(KCl)_5$ and Ar_9 in order to evaluate the relative performance of the models for two different types of potential surfaces. For each system, particular models are found to give results that agree better with simulation than do the results using the simple harmonic approximation. However, no one unparameterized model gives acceptable results for all minima, and the best parameter-free strategies differ for $(KCl)_5$ and Ar_9. Nevertheless, a one-parameter version of one of the models is shown to give the best agreement with simulation for both systems. In an accompanying paper, the best partition function models are used to construct a stochastic master equation which makes predictions of relaxation behavior. These predictions are compared with results from molecular dynamics. © *1998 American Institute of Physics.* [S0021-9606(98)02243-0]

I. INTRODUCTION

For the purpose of studying nonequilibrium thermodynamic processes such as structural relaxation and annealing, the stochastic master equation method has several advantages over molecular dynamics (MD). First, the master equation can take far less time to solve than do the equations of motion over a given time interval and time resolution. The only computationally intensive calculation in the former case is the diagonalization of the transfer matrix, whereas MD studies usually involve an evaluation of pairwise particle distances and the coupled equations of motion at each time step. In addition, the master equation yields a description of average behavior, while many MD simulations are needed to establish a reasonably smooth average. Using a master equation, one can avoid such difficulties as practical limitations on the length of simulations, having to establish the time scale on which ergodicity obtains in a simulation, choosing the length and number of sampling intervals to use, and the time step length to be employed in the simulation. Once the master equation has been constructed, the system behavior can be modeled for different temperatures or temperature histories (or *annealing schedules*) by modifications to the transfer matrix, rather than by obtaining a completely new ensemble of MD trajectories. Another advantage of the master equation is that its transfer matrix is a straightforward product of the theory used to describe the state-to-state kinetics, and also of the underlying potential energy surface (PES). Hence the consequences of specific PES features or changes in the rate theory can be directly observed in the master equation solutions.

In addition to modeling the dynamics of a system, the master equation also yields the equilibrium probability distribution among the n system states, which is identical to the Boltzmann distribution

$$P_i^{\mathrm{eq}}=\frac{Z_i^{\mathrm{M}}\exp(-\beta V_i)}{\Sigma_{j=1}^{n} Z_j^{\mathrm{M}}\exp(-\beta V_j)}. \tag{1}$$

The states of our clusters are the potential wells surrounding local minima on the PES, as discussed in the first section of this paper. In the above expression, Z_i^{M} is the partition function of the individual potential well associated with minimum i, and V_i is the potential energy at the minimum.

In the accompanying paper, we study relaxation using state-to-state kinetics modeled by a stochastic master equation. There, we calculate the elements of its transition matrix using Rice–Ramsperger–Kassel–Marcus (RRKM) transition state theory.[1,2] For a canonical ensemble, this theory requires knowledge of individual reactant and transition state partition functions, where the reactant partition functions are the Z^{M} discussed above. Calculating these partition functions involves the estimation of the size and shape of the catchment basin, or potential well, of each minimum, and the shape of each transition-state region. In this paper, we address only part of the master equation solution: the equilibrium distri-

bution, which is the unique eigenvector of the master equation having zero eigenvalue. To predict this distribution, only Z^{M} need be known, although in some models the transition-state partition functions $Z^{\dagger}$ enter into the expression for Z^{M}. Only Z^{M}, however, can be viably tested via equilibrium simulation, since transition states are not stable stationary points, and thus do not possess a potential well to serve as a natural ''basin of attraction'' which defines the occupation boundary for that stationary point. In this paper, we will only be able to test Z^{M} up to a proportionality constant. This relative test will facilitate an assessment of the absolute magnitudes of Z^{M} and $Z^{\dagger}$ in the accompanying paper.

Z^{M} are traditionally calculated using the harmonic approximation, as used in the harmonic superposition method.[3,4] This method gives the total partition function as the sum of the partition functions for individual minima. Alternatively, the Monte Carlo based multihistogram method[5,6] can be used to determine the partition functions directly from simulation.[7] Another Monte Carlo sampling procedure was suggested by Vieth *et al.*[8] These latter methods avoid harmonic approximations, particularly for temperatures approaching the melting regime. However, these phenomenological approaches are time consuming, and need to be done with care to ensure proper sampling of the potential surface. What we seek as an alternative is an efficient and realistic analytical model for partition functions.

Previous studies of this problem for Lennard-Jones clusters[9,10] used analytic approaches for individual minima that introduced two types of modifications to the usual harmonic approximation: (1) analytical Morse-like anharmonicity terms; and (2) terms to account for transition-state valleys, or flattened regions at and near the transition states leading out of the reactant minima. These methods met with limited success when applied to individual minima, and required either a fitted approximation of the transition-state multiplicity,[9] or adjustable parameters and fits to the averaged properties of subregions on the PES.[10] The partition function of each minimum was then computed from the parameters of the subregion to which it belonged. Where both of these studies were concerned with finding forms for the catchment-basin partition functions that would reproduce caloric curve data, here we will instead focus on a more demanding question: the degree to which the equilibrium population distribution among potential wells P^{eq} can be predicted. The model systems $(KCl)_5$ and Ar_9 were selected because the numbers of minima and saddles on their potential surfaces are small enough to allow us to find all of them and to consider the properties of each minimum individually, yet large enough to have some characteristics of systems too complex to be modeled in full. Our aim is to produce models which can be applied in a statistical manner to larger systems at the level of individual catchment basins. To analyze systems of 20 or more particles, statistical samples of configurations will have to be used. Statistical sampling raises questions about the robustness of model results with respect to changes in sample size and composition, which will be examined in later publications.

In this paper we perform an exhaustive search for all minima and transition states of both $(KCl)_5$ and Ar_9. Using the configurations found, we examine and compare the PES topography and local minimum connectivity of these systems. We then propose several models for calculating partition functions. As a first approximation, we employ the harmonic partition function model. We compare the resulting predictions of the equilibrium probability distributions $P^{eq}(T)$ of locally stable final states to the results of canonical-ensemble MD. We then apply and evaluate various refinements to the harmonic model, based on expected or conjectured features of catchment basins. At this stage, we do not yet address the calculation of transition rates. Rather, we first test the partition function models of minima independent of kinetic effects and of the assumptions built into the master equation. Armed with a reliable partition function model for minima, we then concentrate in the accompanying paper on the effects of transition-state partition functions on transition rate calculations, and on the degree to which these rates, when used to construct a master equation, can predict the simulated relaxation behavior.

II. MAPPING THE PES

In the ''inherent structure'' picture of Stillinger and Weber,[3] for each local minimum there is a catchment basin, or potential well, within which the motion of a system can be described as vibration about the local minimum. For our purposes, each catchment basin is considered to be a state of our system if, in the Markovian sense, the system has a sufficiently long dwell time in that basin to become thermalized in all modes, or, equivalently, that the motion within the basin during the dwell time is ergodic. In this paper we assume that all such catchment basins are ergodic as a first approximation. While simulations indicate that this is likely true for $(KCl)_{32}$ and Ar_{55},[11] the catchment basins of smaller clusters (such as those we study in this paper) are less likely to be ergodic, due to the reduced number of vibrational modes to which internal motions are coupled. When calculating transition rates, transitions may then occur too quickly to establish ergodicity within certain single potential wells. One may then define system states to be the union of potential wells, within which the system remains for a sufficiently long time to behave ergodically.[12]

To predict equilibrium probability distributions, we need the catchment-basin partition functions. It would seem at first to be sufficient to know the details of the local minima. However, many of the partition-function models we use incorporate transition-state and reaction-path information. In addition, since our systematic PES explorations find local minima, saddles, and reaction paths during the same process, we will discuss in this paper not only local minima, but also saddles and the way in which they connect the minima on the PES.

For both $(KCl)_5$ and Ar_9, it is feasible to do an in-depth PES analysis since we can characterize each PES virtually in its entirety. We can then identify and include all important dynamic pathways in the master equation, and thereby study the correspondence between master equation predictions and molecular dynamics simulation. Such a complete description would simply not be possible for a system as large as

$(KCl)_{32}$, for which the number of geometrically distinct minima is estimated to be $\sim 10^{18}$.[13]

In this paper, we consider only transition states which are saddle points of rank one, i.e., those whose Hessians have only one negative eigenvalue. That eigenvalue corresponds to the negative-frequency mode of the reaction coordinate. Considering only rank-one saddles is common in PES studies, based on the supposition that the lowest-energy transition states leading out of a minimum potential well should be rank-one saddles.[14] (However, on some surfaces, lowest-energy saddles need not be of rank one.[15]) For the rest of the paper, we will use the term ''saddle'' to mean a rank-one saddle. Higher-rank saddles could of course not be neglected if there were enough of them to influence the kinetics. In fact, a study of Ar_7 using gradient extremal methods[16] to explore the PES indicates that higher-rank saddle regions can dominate the reaction kinetics at temperatures where the cluster is liquidlike.[17]

A. $(KCl)_5$

Our study of the $(KCl)_5$ PES is an extension of prior work by Rose and Berry with $(KCl)_5$.[18] In their work, Rose and Berry found 15 minima and 17 transition states on the $(KCl)_5$ PES. Our present study extends this earlier work significantly by conducting an ''exhaustive'' systematic search for stationary points. We use the pairwise Born–Mayer potential

$$V_{ij}=\frac{q_i q_j}{r_{ij}}+A_{ij}\exp(-r_{ij}/\rho), \tag{2}$$

with parameters A_{ij} and ρ determined by a fit to alkali halide data by Tosi and Fumi.[19] This set of parameters was used by Rose and Berry and in many other studies.[20]

First, several $(KCl)_5$ configurations were found by quenching via the conjugate gradient method[21] to local minima at points along an MD trajectory. These served as starting points for transition-state searches based on the eigenvector-following (EF) method.[22] At each minimum, searches were started in both directions along the eigenvectors corresponding to the the softest 16 of the 24 normal modes. Extra searches were performed from the softest eigenmode of each minimum by contracting the starting configuration by 0%, 5%, 10%, 15%, 20%, and 25%. Contracting the starting configuration of EF searches in this manner has been shown to increase the number of saddles found from each local minimum.[23] In total, 38 transition-state searches were performed from each minimum found. New minima were discovered by following the steepest-descent path[22,24] downward from the newly located saddle points, which were in turn used to initiate new searches. The configurations we found are a superset of those found by Rose and Berry; we have found a total of 22 geometrically distinct minima (see Fig. 1 and Table I) and 61 geometrically distinct transition states, 50 of which are nondegenerate. Each of the 11 degenerate transition states connects 2 configurations which are permutational isomers with the same geometry and energy.

The set of stationary points we found probably exhausts the actual number of kinetically accessible minima, and probably most or possibly all saddles on the PES. The set of minima we found most likely comprise the complete set of minima which are dynamically sampled at temperatures below dissociation, since many long MD simulations exclusively visited all minima in our set. While molecular dynamics confirms the essential completeness of the sample of minima, it does not yield similar insight about the completeness of the set of saddles found. In general, search methods have more difficulty in finding saddles than in locating minima, since saddles do not correspond to stable stationary points. Nevertheless, given the thorough search for saddles along the normal modes of each minimum, and that the number of unique transition states found reached a maximum after only a small fraction of the total number of searches had been performed, we can assume that we have found most, if not all, of the saddles connecting the minima in our sample. Furthermore, since it is unlikely that a large fraction of transition states associated with a given minimum have eluded our search, we do not expect the overall rates for transitions into or out of this minimum to be greatly affected.

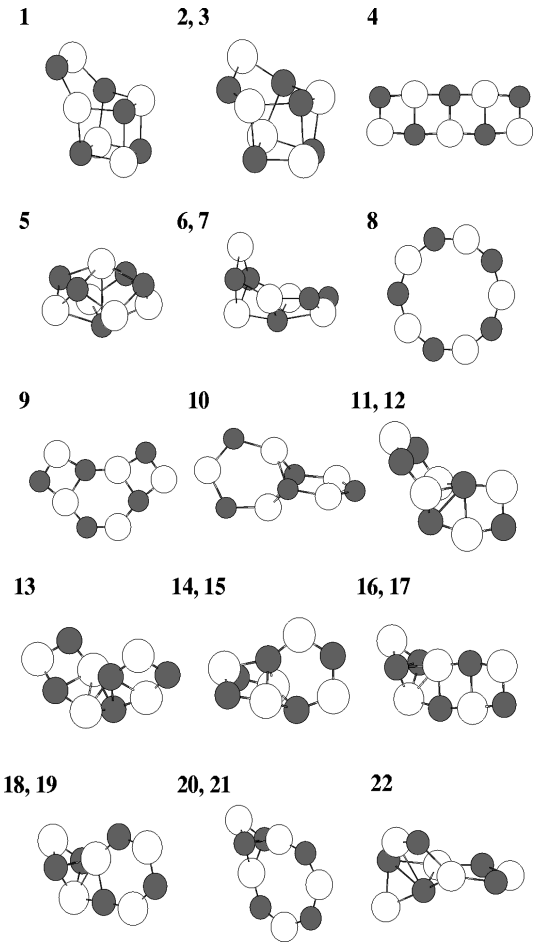

FIG. 1. The 22 distinct locally stable structures of $(KCl)_5$ in order of increasing potential energy. The K^+ ions are shaded. Configuration pairs with nearly identical geometries, but with their K^+ and Cl^- ions switched, are represented in the figure by the lower-energy configuration.

B. Ar_9

The potential energy surface for Ar_9 is given by a pairwise Lennard–Jones potential:[25]

TABLE I. The conformationally distinct minima of $(KCl)_5$. Configuration pairs with nearly identical geometries, but with their K^+ and Cl^- ions switched, are indicated in by matching superscripts a–g.

Minimum	Point group	V (eV/ion)
1	C_s	−3.1244
2[a]	C_s	−3.1116
3[a]	C_s	−3.1115
4	C_{2v}	−3.0979
5	C_{4v}	−3.0970
6[b]	C_s	−3.0907
7[b]	C_s	−3.0906
8	D_{5h}	−3.0868
9	C_s	−3.0670
10	C_{2v}	−3.0661
11[c]	C_s	−3.0635
12[c]	C_s	−3.0631
13	C_1	−3.0622
14[d]	C_s	−3.0615
15[d]	C_s	−3.0614
16[e]	C_s	−3.0591
17[e]	C_s	−3.0591
18[f]	C_s	−3.0549
19[f]	C_s	−3.0548
20[g]	C_{2v}	−3.0482
21[g]	C_{2v}	−3.0476
22	C_1	−3.0476

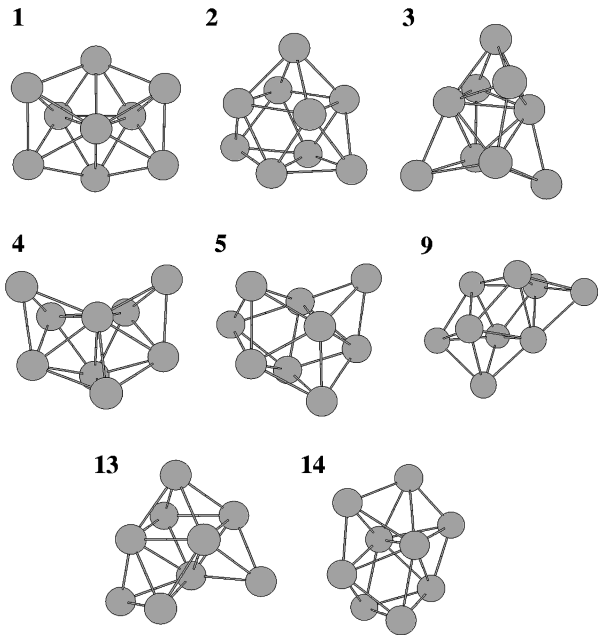

FIG. 2. Selected Ar_9 minima which are either discussed in the text or for which equilibrium data are presented. Configuration indices are in order of increasing energy. Figures for the full set of minima and the 30 lowest-energy transition states can be found in Ref. 27.

$$V_{ij}=4\epsilon\left[\left(\frac{\sigma}{r_{ij}}\right)^{12}-\left(\frac{\sigma}{r_{ij}}\right)^{6}\right], \tag{3}$$

with $\epsilon=1.67\times10^{21}$ J and $\sigma=3.4$ Å.[26] As with $(KCl)_5$, we applied an exhaustive search strategy. Since Ar_9 has a higher saddle-to-minimum ratio than does $(KCl)_5$, we performed a more exhaustive search: one forward and one backward search for each eigenmode and a softest-mode search, at 0% contraction of the starting configuration, and one search along each eigenvalue direction, plus a softest-mode search, using contractions of 8%, 16%, and 24%. For nonzero initial contractions, a backward search yielded the same result as a forward search. In total, 109 unique transition-state searches were performed from each minimum. This search of Ar_9 yielded 21 minima, which correspond in number and energy to the minima found by Tsai and Jordan using the same potential function and a similar EF method.[27] Several Ar_9 minima in particular are discussed in Secs. II C and IV B, and appear in Fig. 2. A total of 156 saddle points were found, 119 of which are nondegenerate. The highest saddle point energy we found was -21.0364ϵ. By comparison, Tsai and Jordan found 152 saddle points, with a higher maximum saddle point energy of -20.178ϵ. All saddle energies they found, except for the highest energy, correspond to saddles in our data set. The five unmatched saddles in our set occur at energies of -22.0012ϵ and higher. The slight discrepancy in the number of high-energy saddles between the two data sets is not surprising, since these saddles are most often found by following the stiffest eigenvector directions. Transition-state searches in these directions tend to have a very low success rate. Since our goal was to do an exhaustive search, we performed a larger number of transition-state searches per minimum, which probably explains why there are more saddles in our data set.

C. PES connectivity

Using the results of our minimum and saddle searches, we now examine the structure and connectivity of each PES. Recent studies[28–31] have addressed the PES structures of Ar and KCl clusters from a statistical approach, in which the elements of the statistical database are ''monotonic sequences'' of local minima on the PES. A monotonic sequence is defined as a sequence of minima, linked by successive transition states, along which each minimum is higher in energy than the one before it. Sets of these monotonic sequences with a common lowest minimum define larger structures or ''basins'' on the PES. In this paper, we will call a basin defined in this manner to be a monotonic sequence basin (MSB). As can be seen from the plot in Fig. 3(a) of all monotonic sequences of $(KCl)_5$, all minima and transition states fall within one MSB; every minimum is connected to the capped-cube global minimum by a monotonic sequence. Hence the important barriers on this surface are not high divides separating large basins, but are simply the saddles between adjacent minima. The MSB whose bottom is the global minimum is termed the *primary* MSB. For Ar_9, all minima except minimum 3 can be reached via monotonic sequences from the global minimum [see Fig. 3(b)]. In the language of monotonic sequences, minimum 3 forms the bottom of a *secondary* MSB, adjacent to the primary MSB. Since only one monotonic step separates minimum 3 from the primary MSB, the inter-basin divide is not distinguish-

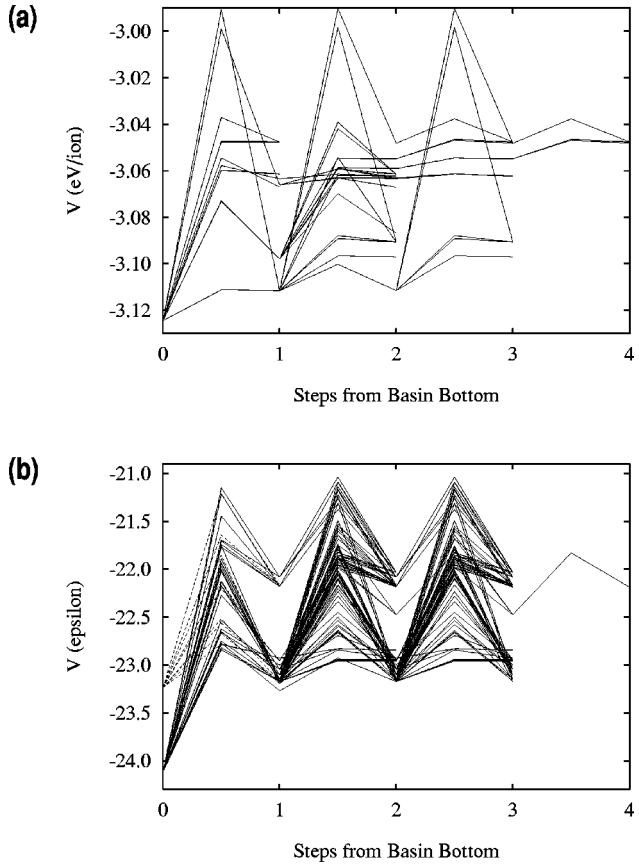

FIG. 3. Plots of all possible monotonic sequences as a function of transition steps away from the bottoms of monotonic-sequence basins (MSBs) for (a) $(KCl)_5$ and (b) Ar_9. For $(KCl)_5$, all such sequences comprise a single monotonic-sequence basin (MSB) with the global minimum (minimum 1) at its bottom. Minima 2, 3, 4, 9, 10, 11, 14, 15, 21, and 22 are directly connected (one step away) from the the global minimum, while 5, 6, 7, 8, 12, 13, 16, 17, 18, 19, and 20 are two steps away. For Ar_9, there are two MSBs. The primary(secondary) MSB is shown in solid(dashed) lines. Note that minimum 3 (at step 0 of the secondary MSB) cannot be reached from the global minimum by a monotonically downhill sequence, and so belongs exclusively to the secondary MSB. Within the primary MSB, minima 11, 13, 15, 16, and 21 are two steps away from the global minimum, while all other minima are directly connected.

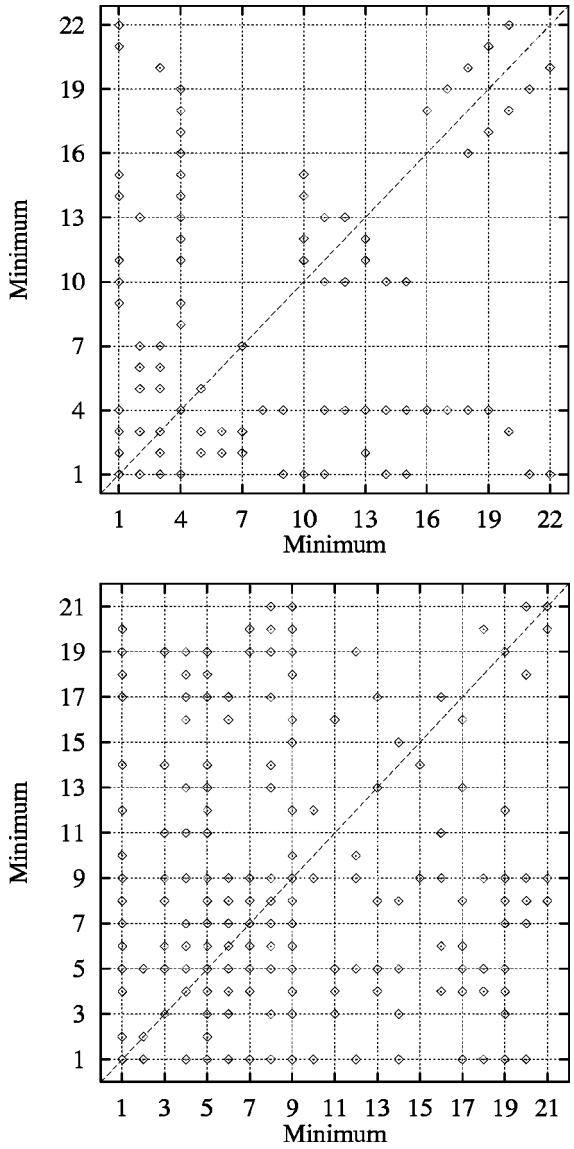

FIG. 4. The connectivity of minima on the PES of (a) $(KCl)_5$ and (b) Ar_9. Each pair of minima connected by one or more transition states is represented with a diamond.

able from a typical transition barrier at that potential energy. The significance of this extra basin on the Ar_9 PES will be examined in the following paper.

The monotonic sequences in the figures also reveal the existence of staircaselike sequences for $(KCl)_5$ and sawtoothlike sequences for Ar_9, as observed in earlier work with larger clusters of these same two types.[28] A staircase sequence exhibits large drops in potential energy in a number of well-to-well steps, indicating the formation of crystalline nuclei. Primary MSBs comprised of sequences with staircaselike profiles have a steep average energy gradient, which has been shown to be an important topographical feature for promoting effective relaxation to basin bottoms and the thermodynamic ground state.[32] A basin with sawtoothlike profiles has a relatively shallow average gradient, and hence lacks the focusing behavior of a staircaselike PES. These transition profiles have been linked directly, via molecular dynamics simulations of relaxation, to whether a system is a focusing ''structure-seeker,'' as in the case of a staircase profile, or a ''glass-former,'' as is the case for a sawtooth profile.[28]

Local minima on the PES are linked by transition states into a network. The connectivity of these networks is illustrated in Figs. 4(a) and 4(b) for for $(KCl)_5$ and Ar_9, respectively. It is apparent that Ar_9 has a higher average number of nondegenerate saddle connections per minimum than $(KCl)_5$. But since not all pairs of minima are connected, and some may be multiply connected, it may be more informative to consider N_C, the number of connected, nondegenerate minimum pairs, which counts a multiply connected pair only once. Let N_M be the number of minima. Then the fractional connectivity C_f, or the average fraction of all other minima to which a given minimum is connected, is given by

$$C_f = \frac{2N_C}{N_M(N_M-1)}. \tag{4}$$

Respective values of N_C for $(KCl)_5$ and Ar_9 are 41 and 75, leading to respective C_f values 0.18 and 0.36. This higher degree of connectivity for Ar_9 is the expected behavior for a Lennard–Jones or other short-range interaction as compared to a long-range ionic potential. In addition, higher values of C_f may correlate with a shallower PES gradient,[33] and consequently with a lack of focusing behavior. Whether this assertion is true for a particular system depends on the height of its barriers. It is also possible in some cases for high connectivity to allow ready passage out of a PES region that would otherwise form a kinetic bottleneck.

III. PARTITION FUNCTION MODELS

For the purpose of modeling real systems, the foundation of the master equation formalism lies in the accuracy of the partition functions used to construct the transfer matrix. Our aim is to identify an easily calculable partition function model, preferably an analytical scheme, that depends only on measurable (or readily computable) properties of the minima and transition states, such as normal-mode frequencies and local derivatives, and which, if possible, minimizes the use of adjustable parameters.

The partition function for an individual minimum i can be written as

$$Z_i^{\mathrm{M}} = n_s Z^{\mathrm{vib}} \times \exp(-\beta V_i), \tag{5}$$

where V_i is the potential energy at the local minimum. The degeneracy factor n_s accounts for the number of distinct permutational isomers, and is given by

$$n_s = \frac{2n_p}{h_s}, \tag{6}$$

where n_p is the total number of nuclear permutations, and h_s is the order of the point group for that configuration.[10] For KCl, $n_p = (N/2)!^2$, while $n_p = N!$ for Ar_9 and other homoatomic clusters. For m vibrational degrees of freedom, the vibrational partition function Z^{vib} is the product of the momentum-space integral $Z_p = (2\pi m*/\beta h)^{m/2}$ (where $m*$ is the mean effective mass of the vibrational modes, and h is Planck's constant) and the configuration integral $\int_{R_i} \times \exp[-\beta \Delta_i V(\mathbf{r})] d\mathbf{r}$ over the catchment-basin R_i of minimum i. In this expression, the potential function is expanded about the local minimum: $V(\mathbf{r}) = V_i + \Delta_i V(\mathbf{r})$.

As a first approximation, Z^{vib} can be calculated within the classical harmonic model:

$$(Z^{\mathrm{vib}})^{\mathrm{Harm}} = \prod_{j=1}^{m} \frac{1}{\beta h \nu_j}, \tag{7}$$

where m is the number of vibrational degrees of freedom in each type of configuration, with $m = 3N-6 = 24$ for minima and $m = 3N-7 = 23$ for transition states. This formalism already vastly improves upon the single-frequency Einstein approximation used in earlier work.[12,29–31]

To make a straightforward anharmonic correction to Eq. (7), we employ an anharmonic model introduced by Haarhoff[34] and adopted by Doye and Wales[10] for application to Ar_{13} and Ar_{55} clusters, which is based on an expansion of the density of states for the Morse potential. We will refer to this method as the Morse analytical (MA) method. In this method, as in the rest of the paper, mode coupling due to anharmonicities will be neglected. With this assumption, Z^{vib}, to first order, is

$$(Z^{\mathrm{vib}})^{\mathrm{MA}} = \prod_{j=1}^{m} \frac{1}{\beta h \nu_j} \left(1 + \frac{a_j}{\beta}\right). \tag{8}$$

The anharmonicity parameter a_j is calculated for the jth mode from the second and third derivatives at the stationary point in the normal mode direction q_j:

$$a_j = \frac{(\partial^3 V/\partial q_j^3)^2}{9(\partial^2 V/\partial q_j^2)^3} = \frac{1}{2D_j^e}, \tag{9}$$

where D_j^e is the depth of the jth Morse potential well.

An obvious shortcoming of the harmonic and MA models is that quantities calculated at a local minimum or transition state cannot be expected to give information about the PES at regions of the potential well far away from the stationary point. For instance, the potential must obviously change curvature and flatten near transition states, due to the finite barrier height. To account for the potential-well broadening near transition states, we use an alternative Morse model which bases anharmonicity parameters on the barrier heights of the reaction paths leading out of a minimum. These barrier heights are closely related to the quantity D^e in the Morse potential; of course, on the actual PES, the limits of each well occur at finite distances from the minimum. This approach has been used by Isaacson *et al.*[35] for modeling the anharmonic force field of potential wells of triatomics, and was investigated by Doye and Wales[10] for Ar clusters. Whereas Doye and Wales used average barrier heights, we employ the actual barrier heights associated with each minimum.

At first, this model may seem plausible only if each transition state can be associated with a normal mode of the minimum, with each reaction coordinate parallel to a particular normal mode. This property will not hold in general, and is certainly impossible when $N_i^\dagger$, the number of transition states leading out of potential well i, is greater than the number of normal modes m. However, Eq. (8) contains the contributions of each normal mode and of the anharmonic corrections for each barrier height as independent factors, allowing us to decouple the reaction coordinates from particular normal modes. Since we already assume that the normal modes of potential wells are uncoupled, this additional assumption should not further compromise the reliability of the model. To account for cases when $N_i^\dagger > m$, we modify the anharmonicity correction in Eq. (8) and obtain

$$(Z^{\mathrm{vib}})^{\mathrm{MB}} = \prod_{j=1}^{m} \frac{1}{\beta h \nu_j} \prod_{l=1}^{N_i^\dagger} \left(1 + \frac{a_l}{\beta}\right)^{\alpha}, \tag{10}$$

where $\alpha = \min(1, m/N_i^\dagger)$, and $a_l = 1/(2\Delta V_l)$, where ΔV_l is the barrier height of the lth transition state associated with the minimum. The product of anharmonic factors in this

equation effectively represents the mean anharmonic contribution per normal mode arising from potential-well broadening due to finite transition barriers. We will refer to this model as the Morse barrier (MB) method.

As outlined by Doye and Wales, Eqs. (8) and (10) derive from a classical approximation of the density of states, which is derived from the quantum expression for the bound-state energies of the Morse oscillator. The partition function that results from taking the continuous Laplace transform diverges. While such divergence is the correct behavior for the classical Morse oscillator, where the dissociation limit occurs at infinity, the classical density of states should remain finite for an isomerization reactant. Hence Doye and Wales adopted the functional form of Eq. (8), which is the Laplace transform of the first-order anharmonic term of the density-of-states expansion. It is important to note that these Morse models will be unphysical for barriers with $\Delta V_l \lesssim kT$. For large anharmonicities, where $\Delta V_l \gtrsim kT$, this term may still be artificially higher than the true anharmonic correction factor. Doye and Wales found that their results using this method were unsatisfactory for this reason.

In the implementation of the Morse models, we have dealt with very low barriers in two ways. The first is to use the anharmonic corrections only for minima that account for most of the equilibrium population. These minima typically lie at lower-energy regions of the PES, and tend not to have very low transition barriers. This selective application of the Morse models (denoted by either MA/S or MB/S) not only helps to avoid low barriers, but also concentrates on accurately modeling the most important catchment basins.

The second approach uses corrections for all modes of all minima, but limits the value of $\eta_l = a_l/\beta$ to a plateau value η_P. We will refer to this method as the MB(η_P) model. A rational maximum value for η_P is 0.5, for which $\Delta V_l = kT$. As η_P is lowered to zero, the anharmonicity is effectively turned off. This model involves a free-parameter fit to the observed data, which can be optimized by the proper choice of η_P. Although this approach compromises our desire to avoid free parameters, we need choose only one parameter for the entire potential surface. The parameter η_P also indicates the relative barrier heights that can be accurately modeled using the Morse models.

If the catchment basin is a relatively steep potential well with a long, flattened transition-state valley (TSV) along the reaction coordinate, the partition function will clearly be underestimated by the harmonic prediction. In order to estimate the partition function contribution from such saddle regions, we followed another method used by Doye and Wales, which models the vibrational partition function for minimum i as

$$(Z_i^{\mathrm{vib}})^{\mathrm{TSV}} = (Z_i^{\mathrm{vib}})^{\mathrm{Harm}} + \sum_{l=1}^{N_i^{\mathrm{TS}}} Z_l^{\mathrm{RC}} \times Z_l^{\dagger}, \tag{11}$$

consisting of $(Z_i^{\mathrm{vib}})^{\mathrm{Harm}}$, the usual harmonic contribution for the catchment basin near the minimum, and an additional contribution from the reaction path TSV associated with each transition state l. The latter contributions are modeled by the ''width'' of the TSV, approximated by the vibrational partition function $Z_l^{\dagger}$ of its transition state, times the ''length'' contribution

$$Z_l^{\mathrm{RC}} = Z_{p_s} \int \exp(-\beta V(s))\, ds \tag{12}$$

from the reaction coordinate s. The momentum-space contribution Z_{p_s} is equal to $(2\pi m_s/\beta h^2)^{1/2}$, where m_s is the effective mass for motion along the reaction coordinate. The integral is taken over s from the saddle point to a distance from the local minimum equal to the geometric mean radius of the harmonic well.

In this paper, $V(s)$ is approximated in two ways. First, by assuming a ''flat'' saddle region, we can set $V(s)$ equal to the transition-state energy $V_l = V_i + \Delta V_l$. In this ''flat'' TSV model (FTSV), we have simply $Z_l^{\mathrm{RC}} = L Z_{p_l} \exp(-\beta V_l)$, where L is the length of the reaction path. The second approach, which we will call the integrated TSV model (ITSV), evaluates $V(s)$ at points along the reaction path as determined from the steepest-descent method of Page and McIver.[22,24] Equation (12) is then integrated numerically over the discrete set of $V(s)$ values.

In an attempt to model the widths of valleys still more realistically, we can compute $Z_l^{\dagger}$ by integrating the numerically calculated potential energy in both directions away from the saddle point along each normal mode, neglecting any changes in the normal-mode directions. We determine the limits of integration by a first pass with the trapezoidal method[21] to determine the point at which the integration should be truncated. This is achieved by monitoring a truncation-error estimation function until its value falls below 10^{-7} of the accumulated integral value. After suitable integration endpoints are obtained, the integral is evaluated directly from a Chebyschev approximation[21] to the integrand using 25 coefficients. This method yields results with an error on the order of 10^{-7} or better, and is many times faster than iterating the trapezoidal method to achieve the same convergence.

As a semi-analytical alternative, we shall also approximate $Z_l^{\dagger}$ by numerically integrating the canonical ensemble integrals for each degree of freedom:

$$(Z_l^{\dagger})^{\mathrm{TA}} = \prod_{j=1}^{m} Z_{p_j} \times \int_{-\infty}^{\infty} \exp(-\beta f_{\mathrm{T}}(q_j))\, dq_j, \tag{13}$$

where Z_{p_j} is the usual momentum-space partition function for the normal mode q_j, and $f_{\mathrm{T}}(q_j)$ is the fourth-order Taylor approximation to the PES in the q_j direction:

$$f_{\mathrm{T}}(q_j) = \frac{k_2}{2} q_j^2 + \frac{k_3}{6} q_j^3 + \frac{k_4}{24} q_j^4, \tag{14}$$

where $k_n = \partial^n V/\partial q_j^n$. This fourth-order scheme, which has proven successful in describing the effect of anharmonicities on protein vibrations,[36,37] was chosen in this work for its flexibility to model both skewness and quartic bend/stretch anharmonicities. Direct observation of the variation of V along normal-mode directions shows that, in general, the

TABLE II. The models used to calculate Z^{vib}. Parameterized models are denoted with an asterisk.

Model		Abbreviation	Z^{vib} expression/Description
Harmonic		Harm	$\Pi_{j=1}^{m}\frac{1}{\beta h\nu_j}$
Morse			
	Analytic	MA	$\Pi_{j=1}^{m}\frac{1}{\beta h\nu_j}\left(1+\frac{a_j}{\beta}\right)$
	MA/S		Apply only to select minima
	Barrier	MB	$\Pi_{j=1}^{m}\frac{1}{\beta h\nu_j}\Pi_{l=1}^{N_i^{\dagger}}\left(1+\frac{a_l}{\beta}\right)^{\alpha}$
		MB/S	Apply only to select minima
		MB(η_P)*	Set $\frac{a_l}{\beta}\leqslant\eta_P$
		MB(η_P)/S*	Combination of MB/S and MB(η_P)
Transition-state valley			$\Sigma_{l=1}^{N_i^{\dagger}}Z_l^{\mathrm{RC}}\times Z_l^{\dagger}$
	Flat		$Z_l^{\mathrm{RC}}=LZ_{p_l}\exp(-\beta V_l)$
		FTSV/H	Harmonic $Z^{\dagger}$
	Integrated		$Z_l^{\mathrm{RC}}=Z_{p_l}\int\exp(-\beta V(s))ds$
		ITSV/H	Harmonic $Z^{\dagger}$
		ITSV/T	Taylor-approximated $Z^{\dagger}$
		ITSV/N	Numerical $Z^{\dagger}$
Taylor approximation		TA	
Numerical		Num	

Taylor approximation to transition-state regions is significantly better than the harmonic approximation for both $(KCl)_5$ and Ar_9.

For comparison, we will also calculate the Z_i^{vib} using the numerical and Taylor approximation (TA) methods, following the same methods as used for $Z_l^{\dagger}$. A summary of all models used in the study is given in Table II.

IV. EQUILIBRIUM PROBABILITIES

The master equation values of P^{eq} can be directly calculated using the Boltzmann expression [Eq. (1)]. In this expression, the partition functions are calculated by our candidate models. To obtain P^{eq} for the actual systems, MD simulations were performed using a canonical-ensemble dynamics method in which stochastic virtual particles simulate an isothermal bath.[38] P_i^{eq} was defined at each temperature to be the average fraction of quenches for which the system was in well i, normalized by the total number of quenches.

As a simple quantitative evaluation of the overall performance of the models at a given temperature we use the L2 norm

$$\xi^{\mathrm{MOD}}(T)=\frac{1}{N_M}\sum_{i=1}^{N_M}(\Delta(P_i^{\mathrm{eq}})^{\mathrm{MOD}})^2, \tag{15}$$

where $\Delta(P_i^{\mathrm{eq}})^{\mathrm{MOD}}=(P_i^{\mathrm{eq}})^{\mathrm{MOD}}-(P_i^{\mathrm{eq}})^{\mathrm{MD}}$, to describe the model error in predicting P^{eq}. We do not divide the terms in the above equation by the variance of the simulation data, since these are typically much smaller than $\Delta(P_i^{\mathrm{eq}})^{\mathrm{MOD}}$. Although the P_i^{eq} must sum to unity, we assume that the data are independent as a simplification. Averaging $\xi^{\mathrm{MOD}}(T)$ over all simulation values of T produces a performance ranking of the models. Tables III and IV give the results for $(KCl)_5$ and Ar_9, respectively.

A. $(KCl)_5$

At each temperature examined, either three or four MD runs were started from each of the three most highly populated minima—the global minimum, rectangle, and decagon (minima 1, 4, and 8, respectively)—as well as from the high-energy minimum 20, for a total of 12–15 runs. Simulations starting from the same minimum were each run from unique, randomly distorted initial configurations. For $(KCl)_5$, we used an MD time step of $\tau=2\times10^{-15}$ s. This time step is 50 times shorter than the shortest vibration periods for $(KCl)_5$ minima and transition states. Each MD run began with 5×10^5 equilibration time steps followed by a series of conjugate gradient quenches. A total of 10^4 quenches were performed in each run, with the quenches spaced 5000τ apart. Testing for correlation effects, we observed that the probability distributions obtained from the MD runs did not change significantly when the quenches were spaced by 1000τ, 5000τ, or $10^5\tau$. The effective temperature range within which MD simulations proved useful lies between 400 K, below which the system was no longer ergodic on the simulation time scale, and 1000 K, above which the cluster would fragment into two subclusters.

The simulations indicate that the global minimum, rectangle, and decagon dominate the probability distribution (see Fig. 5). In the temperature range between 500 and 600 K, the most probable structure shifts from the global minimum to the two planar structures. This behavior is in agreement with

TABLE III. Errors $\xi^{\mathrm{MOD}}\times 10^5$ for select models applied to $(KCl)_5$. In the MB(η_P) model, $\eta_P=0.1$.

T	MB(η_P)	MB/S	FTSV/H	Harm	ITSV/H	TA	ITSV/T	Num	ITSV/N	MB
400	2.8	5.4	5.7	4.9	431.0	14.9	6.8	15.7	9.1	250.8
450	21.4	40.3	32.7	35.6	217.8	104.1	64.0	109.6	84.2	396.5
500	37.7	74.0	67.3	74.8	137.1	259.7	164.4	276.3	229.5	545.4
550	73.0	134.9	136.0	155.6	156.4	546.0	377.4	583.2	534.5	660.7
600	39.7	86.4	128.3	151.1	228.4	612.9	459.7	665.4	691.3	777.3
650	33.9	71.5	174.3	212.7	300.6	715.7	605.5	783.3	932.8	940.8
700	22.4	45.4	212.3	273.7	370.8	703.6	687.7	777.5	1081.9	1215.1
750	15.1	28.2	259.5	358.4	426.7	665.6	736.2	741.8	1178.8	1626.7
800	11.6	19.0	296.8	443.9	479.3	608.5	747.7	683.9	1211.9	2087.0
850	9.8	17.9	329.2	534.8	519.2	581.2	755.4	657.0	1233.5	2522.9
900	7.6	17.2	367.7	639.8	531.8	557.2	703.9	634.8	1172.6	2867.0
1000	7.5	32.7	380.7	772.5	579.5	558.0	661.0	639.3	1101.1	3361.6
Avg	23.5	47.7	199.2	304.8	364.9	494.0	497.5	547.3	788.4	1437.6

the MD work done by Rose and Berry to determine the solid–liquid transition for the $(KCl)_5$ system.

In Fig. 5, the harmonic-model values of P_i^{eq} for the ten lowest-energy minima are compared to simulation values. Although for both cases P^{eq} shifts as expected to higher-energy minima with increasing temperature, their quantitative results are quite different. The largest disparities involve the rectangle and the decagon. At higher temperatures, simulations indicate that the rectangle always dominates P^{eq}, whereas the harmonic model predicts that the dominance should switch from the rectangle to the decagon above 525 K. These discrepancies are not surprising, considering the simplicity of the harmonic theory. Near saddle points and in other regions which have one or more negative frequencies in their instantaneous normal-mode (INM) spectrum, the surface is certainly far from harmonic.

As a first attempt to model these anharmonicities, we employed the MA model. The sparsely populated high-energy minima have very large anharmonicities in some degrees of freedom, rendering the MA model unphysical. We discounted these anharmonicities from the model, applying the MA expression only to minima with smaller a_j values (the MA/S model). Although the model produced a slight upward shift in the value of P_4^{eq} and a corresponding downward shift of P_8^{eq} with respect to the harmonic model, the agreement with simulation values was effectively no better. The anharmonic factors for the more highly populated minima were too small to make a significant improvement over the harmonic model. For this reason, we do not present the MA/S results with those discussed below.

We next turned to TSV models to estimate the anharmonic PES features. Since the rectangle and decagon dominate P^{eq} at high temperatures, and the values P_1^{eq} and $P_4^{\mathrm{eq}}+P_8^{\mathrm{eq}}$ given by the harmonic model are approximately equal to their simulation counterparts, we hypothesized that the most important anharmonicities were concentrated in the rectangle-decagon region of the PES. Since these two minima are connected by only one transition state, we further assumed that there is a highly populated TSV on the rectangle side of the transition state. These hypotheses were justified by an examination of the decagon-to-rectangle reaction path. On the decagon side of the path, the energy corresponds closely to that of the harmonic approximation to the softest vibrational eigenmode over most of the path. In contrast, the energy profile of the rectangle side of the path is quite nonquadratic, has negative curvature over most of its length, and is significantly broader than the mean harmonic well. It is then possible that a significant region of the PES is not accounted for by the harmonic model, which would then underestimate the density of states in the rectangle catchment basin, and hence in P_4^{eq} as well.

Using the FTSV model with harmonic approximations to

TABLE IV. Errors $\xi^{\mathrm{MOD}}\times 10^5$ for select models applied to Ar_9. In the MB(η_P) and MB(η_P)/S models, $\eta_P=0.1$.

T	MB(η_P)/S	TA	Num	MB(η_P)	ITSV/H	Harm	FTSV/H	ITSV/N	MB/S	MB	ITSV/T
16	1.3	0.6	0.6	2.5	34.7	1.4	14.6	308.1	13.5	38.4	1414.2
17	1.7	1.9	2.0	4.2	51.4	3.5	32.9	310.5	30.8	84.6	1780.9
18	2.2	4.5	4.7	6.7	65.5	7.6	64.3	296.2	64.0	161.3	1851.1
19	4.0	7.5	7.8	12.1	78.3	15.6	115.4	276.2	125.6	278.5	1774.9
20	5.2	13.1	13.5	17.3	77.0	28.4	169.7	243.5	209.2	408.8	1594.5
21	7.1	18.5	19.2	24.2	69.6	46.6	225.2	210.7	322.3	546.4	1393.4
22	8.1	27.7	28.7	29.5	50.9	70.7	256.7	167.0	439.2	650.4	1162.4
23	11.3	32.0	33.0	39.4	39.8	101.9	290.0	142.4	588.6	760.7	985.6
24	14.4	39.4	40.4	48.5	26.7	140.0	297.7	213.1	725.2	830.2	812.0
25	18.8	41.5	42.2	60.0	19.4	181.9	307.3	386.3	889.9	909.1	695.9
26	20.4	50.5	51.1	64.3	10.1	221.5	277.6	454.1	999.0	921.7	561.3
Avg	8.6	21.6	22.1	28.1	47.6	74.5	186.5	273.5	400.7	508.2	1275.1

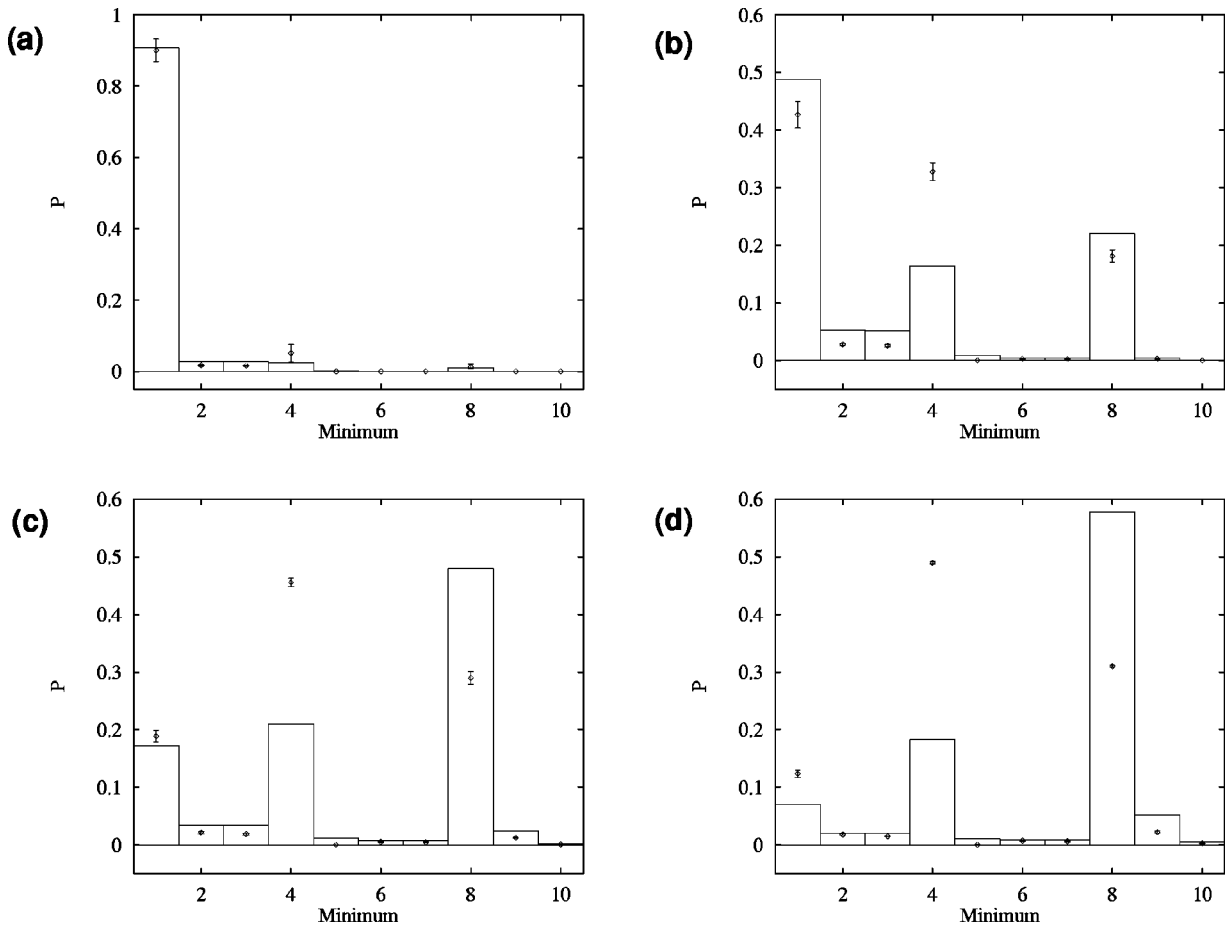

FIG. 5. Comparison of the harmonic model (boxes) versus MD values (points with error bars) of P_i^{eq} for the ten lowest-energy $(KCl)_5$ minima at (a) 400 K, (b) 600 K, (c) 800 K, (d) 1000 K.

$Z_l^{\dagger}$ (FTSV/H), we estimated the relative occupation probabilities of the harmonic potential wells with respect to the transition state valleys. At 200 K, the transition-state regions contain about 10^{-4} of the total probability. At 600 K, this number increases to 0.1, and climbs to 0.27 at 1000 K. In Fig. 6, we compare the results for P_i^{eq} for this and other models against the MD results for selected $(KCl)_5$ minima as a function of temperature. Figure 6 indicates that, although this approximation scheme gives better probabilities than the MA model, it is still unable to reproduce the simulation values.

To account for the actual reaction-path energy profile, and to increase the TSV density-of-states contribution, we applied the integrated TSV model, approximating $Z_l^{\dagger}$ harmonically (ITSV/H). While this model predicts the high-temperature dominance of the rectangle, it drastically overcounts its probability. This model could not be used below 350 K, since in that regime it gave the unphysical result of a nondecreasing population for the rectangle. In addition, this model always attributes more than 90% of the probability to TSVs for temperatures up to 1000 K, with a slightly declining probability as temperature increases. This behavior is also unphysical, since the potential wells of the minima should ultimately dominate at sufficiently low temperature. This model clearly overestimates the influence of any TSV features on the PES and overwhelms the harmonic potential-well partition functions, and hence is not a viable model choice.

We attempted to correct this overestimation by modeling the TSV width differently. By inspecting one-dimensional profiles of the PES along normal-mode directions leading away from transition states, we found that, on the average, the vibrational modes of the saddle points were stiffer than their harmonic approximations. Deriving $Z_l^{\dagger}$ by numerical integration, we find that this stiffening leads to values consistently smaller than $(Z_l^{\dagger})^{\mathrm{Harm}}$ by factors predominantly in the range 1.5–4. For some saddles, this factor is 10 or higher. These modified $Z_l^{\dagger}$ lower the TSV probability.

Incorporating the numerical estimates of $Z_l^{\dagger}$ into the ITSV model (ITSV/N), we recover the proper low-temperature behavior. The TSV occupation probability is now more plausible, with 6×10^{-4} of the total probability at 400 K. The probability grows to 50% at 420 K and reaches 97% at 1000 K. However, this model overweights the global minimum, and the results start to diverge from the MD results at 400 K, growing worse with increasing temperature. Using Taylor-approximated $Z_l^{\dagger}$ in the model (ITSV/T) yields similar results for most minima, except that P_4^{eq} is increased at the expense of P_1^{eq}, bringing these two probabilities into fortuitously better agreement with simulation.

A possible problem with TSV models in general is that,

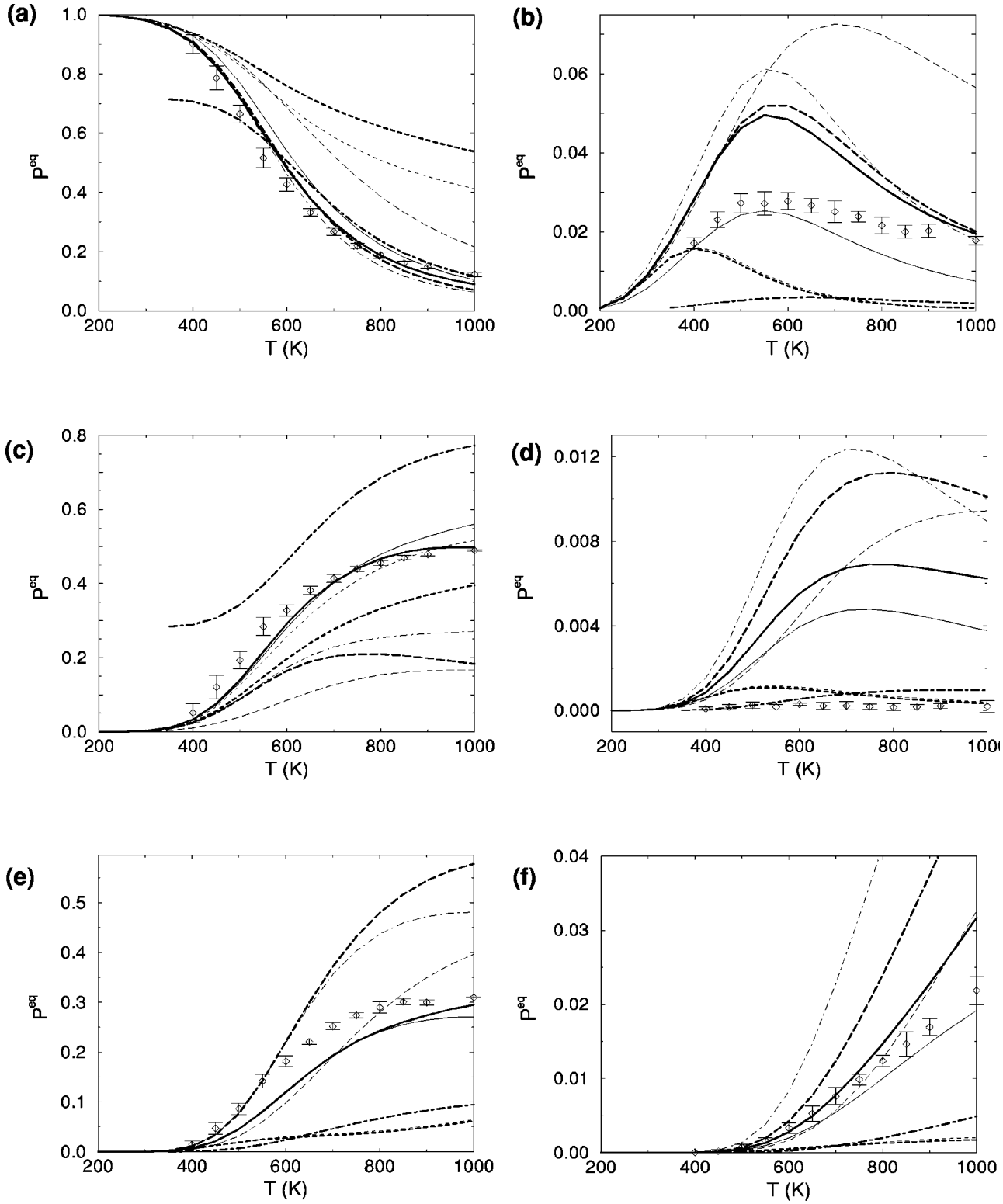

FIG. 6. Comparison of model values of P_i^{eq} to MD results for $(KCl)_5$ minima (a) 1, (b) 2, (c) 4, (d) 5, (e) 8, and (f) 9. Error bars for the MD data are the standard deviation over simulation runs. Models: Harmonic (thick long dashes), TA (thin long dashes), FTSV/H (thin dot-dash), ITSV/H (thick dot-dash), ITSV/T (thin short dashes), ITSV/N (thick short dashes), MB (thin solid line), MB($\eta_p = 0.1$) (thick solid line).

for a given PES, the notion of a TSV may not be a realistic model of anharmonic features. Even if it is, the assumptions made about TSV topography may be too simple to attain an accurate quantitative estimates of P^{eq}. However, the results were not particularly sensitive to the choice of the TSV cutoff where it meets the minimum well, perhaps due to the relatively small mean radii of the harmonic potential wells of local minima compared to the lengths and multiplicities of TSVs.

We then tested the MB model to see if it could model anharmonicities more faithfully than the TSV models and more significantly than the MA/S model. As mentioned pre-

TABLE V. $(KCl)_5$ basin crossover temperature T_C for the MD results and nine models.

Model	T_C (K)	Model	T_C (K)
MD	590	ITSV/H	610
Harm	650	ITSV/T	825
MB/S	645	ITSV/N	$\gtrsim$1100
MB($\eta_P=0.1$)	640	TA	845
FTSV/H	645	Num	850

viously, we must take into account the problems that low transition barriers cause for Morse models. Since most of the minima on the $(KCl)_5$ PES have at least one such barrier, we used the MB model only for the global minimum, rectangle, and decagon. These are the most important minima, none of which have low barriers. From Fig. 6 it can be seen that this model makes a significant improvement in predicting the P^{eq} distribution. P_4^{eq} and P_8^{eq} are now in correct proportion, but P_1^{eq} is somewhat too large. Above 750 K, this overestimation diminishes and disappears by 1000 K, by which point P_4^{eq} is too high and P_8^{eq} is too low.

We also applied the MB(η_P) method, which uses the anharmonicity plateau η_P. Upon adjusting the value of η_P we found the overall best fit to the MD data with η_P in the approximate range 0.08–0.10, significantly lower than the heuristic value 0.5. We include the results for P^{eq} with $\eta_P=0.1$ in Fig. 6. Of particular note, P_1^{eq} is systematically lower than for the MB model, and is closer to the MD results well into the liquidlike range of temperature. In addition, the high-temperature behavior of P_4^{eq} is slightly improved. Since minima 1 and 4 have many more transitions than do other minima, it is likely that the MB model weights the transition-state regions associated with them much more heavily than for other minima. In this case, η_P may help adjust the growth of the anharmonicity factors with increasing temperature in the MB model to match the real growth in importance of anharmonic PES regions.

The $P_i^{eq}(T)$ curves for the numerical and TA models are very similar, differing only slightly for the larger P_i^{eq} with increasing temperature. For clarity, we plot only the TA results. Although the curves have the correct functional behavior, P_1^{eq} is significantly higher than in the MD results, and lies outside the distribution of other well-behaved models (excluding the ITSV models). In addition, P_4^{eq} is lower for these models than in any other model, with P_8^{eq} becoming dominant at high temperatures.

In the next paper, we discuss the global structure of the $(KCl)_5$ PES, and show that the global minimum and the three-dimensional structures 2, 3, 5, 6, and 7 belong to one dynamically linked basin, while the planar rectangle, decagon, and minimum 9 belong to a separate basin. Essentially all of the occupation probability is concentrated in these two basins. We can then use the crossover temperature T_C at which the occupation probabilities of these two basins cross over as an additional test to our models. Values of T_C are given in Table V. This quantity may prove useful for judging model effectiveness in relaxation studies, since the interest in such a case may be to study the relaxation to a basin associated with a general structure type, instead of a particular structure. We note that T_C is systematically higher for the numerical and TA models. This observation is consistent with our examinations of potential well morphology, which indicate that their normal-mode profiles tend to be stiffer on the average than their harmonic approximations, leading to relatively lower occupation of higher-energy regions on the PES at a given temperature.

Of all models examined, we find that the MB($\eta_P=0.1$) model gives the best overall agreement with MD results for $(KCl)_5$. The MB/S model results, however, are reasonably close to those of MB($\eta_P=0.1$). Hence, if desired, the use of free parameters can be avoided when modeling partition functions, and only information about the minima, saddles, and reaction paths is needed.

The next best model is FTSV/H, whose performance is significantly lower than that of MB/S and MB($\eta_P=0.1$). It provides a slight improvement over the harmonic model. Since its perturbation from the harmonic model is small, it is well behaved, and suffers from the same growth in discrepancies as a function of temperature. The ITSV, numerical, and TA models, on the other hand, have significantly worse agreement with simulation than does the harmonic model.

B. Ar_9

For Ar_9, we used the same MD method as for $(KCl)_5$ with a time step of $\tau=3\times10^{-15}$ s. Each run was equilibrated for 5×10^5 time steps before quenching. Simulation temperatures ranged from 16 K to 26 K in 1 K intervals. For all temperatures, an equal number of MD runs were started from each of minimum 1 (the global minimum), 5, 10 and 16. At both 16 and 17 K, a total of four simulations were run, with 2×10^4 quenches performed at intervals of $10^4\tau$. For each higher temperature below 26 K, a total of 12 MD runs were performed. At 26 K, the cluster would frequently dissociate within the simulation time. The data at this temperature are from five runs that completed with the cluster still intact. Up to 22 K, a quench interval of $10^4\tau$ was used, while 5000τ was used above 22 K.

As shown in Fig. 7, the global minimum of Ar_9 always dominates P^{eq}, its probability remaining above 50% even as the dissociation temperature is reached. Minimum 5, with C_1 symmetry, is the next most probable, followed by other minima in the 3–9 range. With increasing temperature, P_9^{eq} quickly grows from being the lowest probability of this group of minima to being the highest. The probability of minimum 2 is strikingly low, in part because its relatively high D_{3h} symmetry reduces its permutational degeneracy on the PES (see Fig. 2).

From the comparison in Fig. 7 of harmonic P^{eq} values to simulation results for two selected temperatures, it is apparent that minima 3–9 are somewhat undercounted and minima 11–15 are overcounted by the harmonic approximation. For minima 5 and 9, the approximate probability is especially low, while P_{13}^{eq} is approximately 20 times greater than the simulation result. At 18 K, the harmonic and MD values of P_1^{eq} agree to within 1%. By 26 K, $(P_1^{eq})^{Harm}/(P_1^{eq})^{MD}$ decreases to 0.86. Most notably, $(P_i^{eq})^{Harm}/(P_i^{eq})^{MD}$

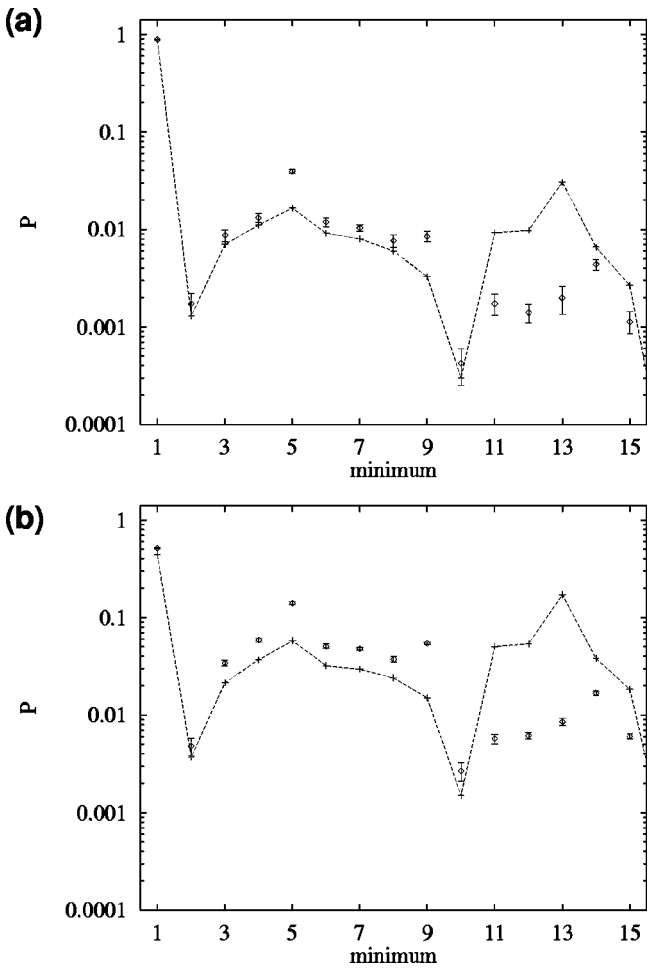

FIG. 7. Comparison of the harmonic model (crosses and dashed line) versus MD values (points with error bars) of $\log_{10} P_i^{eq}$ for the 15 lowest-energy Ar_9 minima at (a) 18 K and (b) 26 K.

decreases smoothly for minima 3–9 and smoothly increases for minima 11–15. Furthermore, these changes are roughly uniform over the members of each group. From these observations we make the following hypotheses: (1) each of these sets likely corresponds to a PES basin whose members have potential wells with a characteristic type and degree of anharmonicity, and (2) none of the Ar_9 minima have unique features, such as the TSV regions introduced above, that are large enough to be significantly populated.

The potential energy profiles of potential wells along normal-mode directions show that, for minima 11–15, the softest normal-mode profiles are significantly stiffer with respect to the harmonic approximation than are the modes of minima 3–9. Such stiffness is often associated with bending modes. The softest-mode numerical profiles of minima 1–5 are nearly harmonic, and only minima 6 and 9 have the same high stiffness that characterizes the softest modes of minima 11–15. In general, a larger fraction of the normal-mode profiles of the 11–15 set have large negative anharmonicities. Hence it appears that the harmonic model predicts potential wells for minima 11–15 that are too broad, thus overestimating their partition functions and causing a systematic increase in P_i^{eq} for these minima, and a corresponding decrease for minima 3–9.

A comparison of model P_i^{eq} values to the simulation results for Ar_9 is given in Fig. 8. We display results for the global minimum ($i=1$), a representative from the 3–9 set (minimum 4) and the 11–15 set (minimum 14), plus minima 5, 9 and 13, whose $(P_i^{eq})^{Harm}$ values show the most deviation from the MD results. Figures of these minima appear in Fig. 2.

As in the case of $(KCl)_5$, the MA model made no significant modification to the harmonic model P_i^{eq} values. In contrast to $(KCl)_5$, it is worth noting that the anharmonicities a_j in this model were small for all minima except for minimum 13.

Given our hypothesis about the absence of important individual TSV features, we would not expect the TSV models to be good candidates. We note that the FTSV/H model is actually able to improve agreement for minima 4, 5, and 9, but is much worse than the harmonic approximation for minima 1, 13, and 14. This increased deviation from simulation may stem from the fact that, according to our observations for both $(KCl)_5$ and Ar_9, the reaction paths leading from a transition state tend to be longer on the side leading to the higher-energy minimum. Since the FTSV model assumes that TSVs are flat, it weights the TSVs only by length, causing high-energy minima to be weighted even more than in the harmonic model. The ITSV/H model, which gives weight to the energy along the reaction path as well, tends to improve upon the FTSV/H results at high temperatures. Surprisingly, the ITSV/H model gives the overall best agreement with simulation for analytic, parameter-free models. In addition, the low-temperature probability is correctly dominated by the global minimum [in contrast to the results of the same model used with $(KCl)_5$].

We note, however, that the ITSV/N model applied to Ar_9 yields $P_i^{eq}(T)$ profiles that vary with temperature in an irregular manner (exhibiting too many inflection points), and also yields particularly low values of P_1^{eq} at low temperatures. The ITSV/T model exhibits the same unphysical variation in the $P_i^{eq}(T)$ profiles, and has even worse overall performance than does ITSV/N.

Although one or more of the TSV models may work well with a particular cluster, predicting *a priori* which ones will work may not be possible. The only ''safe'' model in this case would seem to be the FTSV model, which adds a relatively small contribution to the potential-well density of states. However, this model is likely only to work when it is necessary to account for specific minima which have a large number of reaction paths leading out of them, with a correspondingly large anharmonicity. For surfaces without such minima, the FTSV model is likely to only exacerbate the inaccuracy of the harmonic model.

As with $(KCl)_5$, we tried the MB models for Ar_9. Since some transition-state barrier heights for minima 11–15 have very high values of η_l, we have found it necessary to use an MB/S model which excludes anharmonic corrections to the partition functions of these minima. The main problem with this model is that P_5^{eq} becomes far too large, forcing P_1^{eq} to fall increasingly short of the simulation results. This occurs because the 29 reaction paths leading out of minimum 5 have

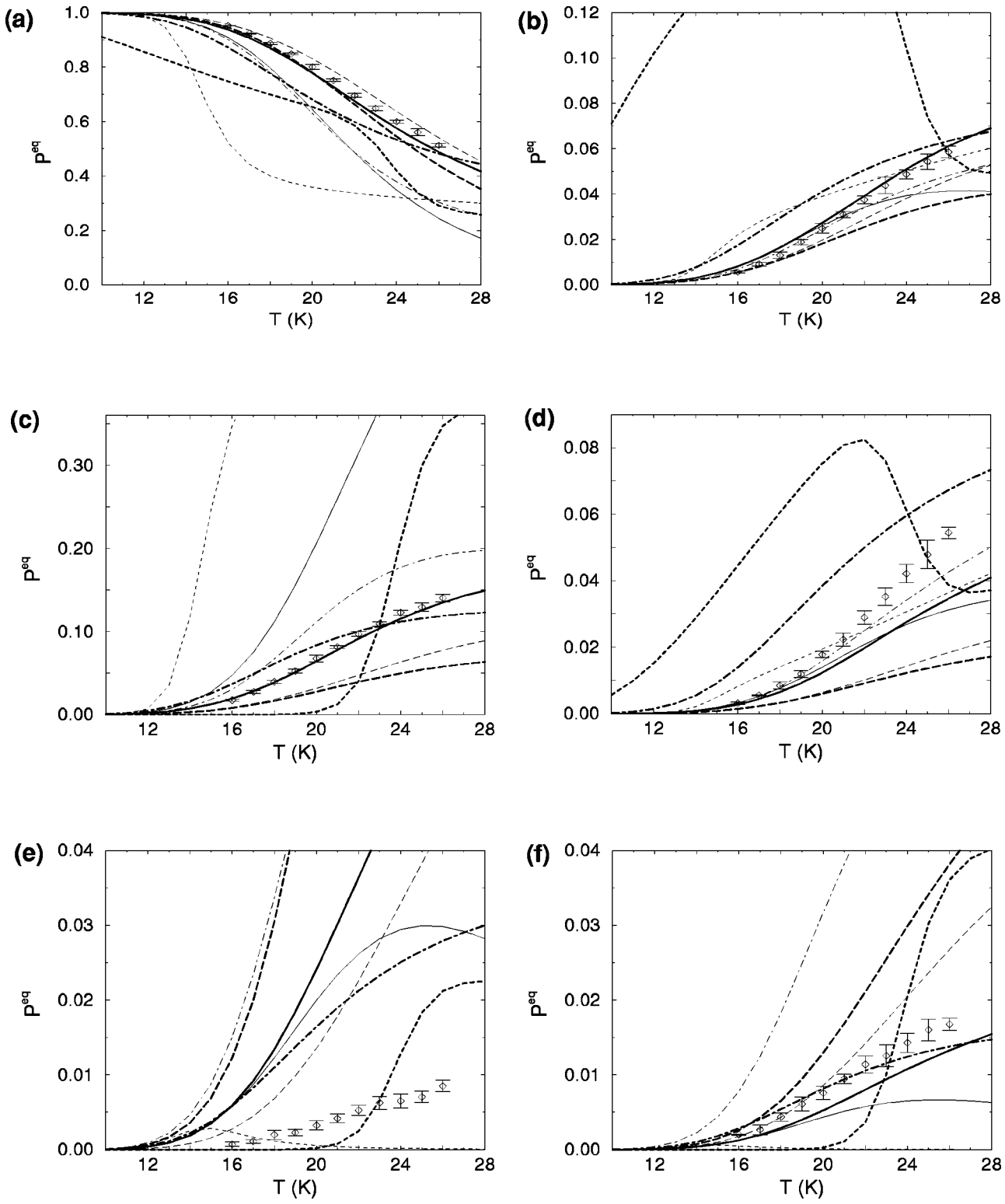

FIG. 8. Comparison of model values of P_i^{eq} to MD results for Ar_9 minima (a) 1, (b) 4, (c) 5, (d) 9, (e) 13, and (f) 14. Error bars for the MD data are the standard deviation over simulation runs. Models: Harmonic (thick long dashes), TA (thin long dashes), FTSV/H (thin dot-dash), ITSV/H (thick dot-dash), ITSV/T (thin short dashes), ITSV/N (thick short dashes), MB (thin solid line), MB($\eta_P = 0.1$)/S (thick solid line).

significantly lower transition barriers than do the 34 reaction paths leading out of the global minimum.

To improve the MB/S model, we adjusted the plateau value η_P as we did for $(KCl)_5$. Although this family of models prevents unphysical correction factors, they overestimate P_i^{eq} for minima 11–15 by as much as a factor of 3 at high temperatures. We have opted to exclude the anharmonic contributions for minima 11–21, noting that P_i^{eq} results for minima 1–10 are not significantly changed whether or not they are excluded. In general, when partition functions of minima (such as minima 11–15) are systematically overestimated by the harmonic approximation, the anharmonic ad-

TABLE VI. Ar_9 basin crossover temperature T_C for the MD results and nine models.

Model	T_C (K)	Model	T_C (K)
MD	26.2	ITSV/H	25.2
Harm	24.8	ITSV/T	16.2
MB/S	21.8	ITSV/N	23.2
MB(η_P=0.1)/S	25.7	TA	26.9
FTSV/H	21.8	Num	27.0

justment made by MB models will only increase the discrepancy. Identifying such minima may require a preliminary examination of the MD P^{eq} distribution compared to harmonic or MB model calculations. We will call this combination of the MB/S and MB(η_P) approaches the MB(η_P)/S model.

This model fits the simulation data well, especially for minima 1 and 5, with the same plateau value $\eta_P=0.10$ that was used for $(KCl)_5$. Performing the fit at 25 K, the range of η_P that fit minimum 5 within the simulation error bars was determined to be 0.099–0.107, and 0.077–0.089 for the global minimum. The only minimum for which the model works poorly is minimum 13. As previously noted for $(KCl)_5$, since η_P can be freely chosen to limit the growth of anharmonic effects in the model to match the real growth, the good agreement we achieve with the MB(η_P)/S model is not surprising. On the other hand, it is noteworthy that the optimal value η_P should be approximately the same for both clusters we studied. This value may indicate a general anharmonicity range for which the MB class of models is reasonably accurate. Such a conclusion is left for future work.

For Ar_9, the numerical and TA models gave essentially identical results. The P_i^{eq} profiles of these two are represented in Fig. 8 by the TA results. For P_1^{eq} the results are in very good agreement with the simulation data. For minima 5 and 9, these models underestimate P_i^{eq}, and do not make significant improvement over the harmonic model. They do much better for the higher-energy set of minima, and they significantly reduce the harmonic-model overestimation of P_{13}^{eq}. In general, these models perform better than the MB/S, harmonic, and all TSV models.

The difference in quality of the numerical and TA results for the two clusters may be due to an extra degree of twisting of the reaction paths of $(KCl)_5$. Our observations of the potential surfaces did not indicate any clear tendency of the normal modes and reaction paths of $(KCl)_5$ to be more ''twisted'' than those of Ar_9. However, the reaction paths of Ar_9 might correspond more closely to normal modes, since the short-range Lennard–Jones interaction is more likely to limit isomerization mechanisms to simple distortions along vibrational modes, whereas the long-range interactions in $(KCl)_5$ may result in more complicated relationships of the reaction paths to normal modes. As a result, the density-of-states near transition states is likely to be poorly modeled by the numerical and TA methods.

We show values of T_C for Ar_9 in Table VI. For Ar_9, we select T_C to be the point at which P_1^{eq} drops below 0.5. Once again, models which are closer overall to reproducing simulation results have correspondingly similar values of T_C. Where for $(KCl)_5$, stiffening of transition-state normal modes caused T_C to occur at higher values, for ITSV/N models it is slightly lower, and for ITSV/T it is extremely so. This reverse behavior is likely due in large part to the unpredictable properties of these models, but also because the majority of normal modes of Ar_9 transition states are nearly harmonic, unlike $(KCl)_5$.

Reviewing the models, we find that as for $(KCl)_5$, the MB(η_P) model most faithfully reproduced the P^{eq} simulation results. Unlike the case for $(KCl)_5$, the MB/S model is not as good an approximation. In fact, the numerical, TA, ITSV/H, and even the FTSV/H model are better than the MB model overall. The ITSV/H model is in fact the best parameter-free model for Ar_9. We note that the TSV model results do not indicate that any one model of $Z^{\dagger}$ works well for all system types. Additionally, we find that the numerical and TA approximations give the second-best agreement with simulation for Ar_9, where for $(KCl)_5$ their results were less accurate overall compared to the harmonic approximation.

V. CONCLUSIONS

The minima, transition states, and connectivity information have been obtained for the $(KCl)_5$ and Ar_9 potential energy surfaces. Normal modes and frequencies have been determined for the minima and transition states. In addition, numerically derived third and fourth derivatives have been calculated. This information was used to calculate partition functions for local minimum potential wells.

Comparing the equilibrium probability distributions predicted by these partition functions with molecular dynamics results shows that the harmonic approximation systematically under- or overpredicts the partition functions, because this model fails to account for the positive anharmonicities near transition-state regions, as with $(KCl)_5$, or, as in Ar_9, to represent the characteristic negative anharmonicities of minima in a particular region of the PES.

Of the TSV family of models, it appears that the FTSV/H model can improve somewhat upon the harmonic model by taking into account the many TSVs of highly populated minima, but only if there are one or more other highly populated minima with few transition states. This is the case for $(KCl)_5$, but not for Ar_9. In the latter case, the added TSV state densities added to each potential well tend to compete with one another, negating any benefit of the model. In addition, it is unlikely that an FTSV model can reliably predict the actual value of the partition function, a fact that will be important for transition-state theory calculations.

Of ITSV models, only the ITSV/H model for Ar_9 works better than the harmonic model. For $(KCl)_5$, this model has unphysical low-temperature behavior. In neither case are the ITSV/T or ITSV/N models viable alternatives to the harmonic model. In general, the ITSV models tend to add large contributions to the density-of-states of a potential well that overwhelm the harmonic contributions. Since these TSV contributions are very simply modeled, the ITSV models are prone to inaccuracy and unpredictable behavior. Furthermore, the ITSV/N and ITSV/T may be unreliable due to the

difficulty of defining the width of the TSVs when numerically integrating $Z_l^{\dagger}$ in Eq. (11), or when using Eq. (13). In the latter case, there may be cases where the polynomial extrapolation given in Eq. (14) is too shallow, or turns over.

Of all parameter-free models, the MB/S method has the best overall performance for $(KCl)_5$, but was poor for Ar_9. For both systems, the performance of this model can be increased by introducing a parameter η_P that limits the maximum anharmonicity contribution of any given barrier height. This parameter has approximately the same optimal value for both $(KCl)_5$ and Ar_9. Furthermore, this MB(η_P) model yields the best agreement with the simulation values of P^{eq} for both systems. As a further improvement upon Ar_9 results, the anharmonic contributions of high-energy ''problem'' minima were excluded. This hybrid MB(η_P)/S model improved agreement with simulation even further.

The success of an MB class model can be improved by excluding certain minima which have low transition barriers. In practice, these barriers can be easily identified (based on, say, their size relative to k_BT), and those minima associated with them can then be roughly approximated by the harmonic model. Typically, minima with a significant occurrence of such barriers have shallow potential wells. Such wells occur primarily at high potential energies, and their occupation probability will be severely Boltzmann attenuated. In some cases, however, high-probability potential wells, while relatively deep overall, may possess one or a few low transition barriers. In general, this event is unlikely for low-energy cluster minima. Nevertheless, in the case that two or more highly occupied minima are interconnected by low barriers, it would be more realistic and practical to treat this group of minima as a single reactant state when used in the master equation. This approach, while requiring modification to the partition function expression, obviates the low-barrier problem and helps to ensure that ergodicity can be attained within the reactant well, a necessary condition for Markovian master equation dynamics.

As a comparison to our analytic and semi-analytic methods, we used direct numerical integration to evaluate the partition functions, over both numerically calculated and Taylor approximated potential well profiles. In the case of Ar_9, these models prove to be the next-best alternative to MB(η_P), while they fail for $(KCl)_5$, due to poor correspondence of normal modes with reaction paths.

Our results indicate that there is no one parameter-free model that works well with both types of systems. The MB(η_P) model may then be ideal for general application, and for some systems may not be avoidable. Although it requires some phenomenological data to determine η_P, this relatively simple model could be competitive with more complicated anharmonic corrections to the partition functions involving fits to caloric simulation data. In practice, it may be possible to use a nominal value of η_P (perhaps, as we found, $\eta_P \approx 0.1$) as a reasonable approximation for a large range of systems. The MB($\eta_P=0.1$) and MB($\eta_P=0.1$)/S models will be adopted as optimal models for $(KCl)_5$ and Ar_9, respectively, in the following paper on the kinetics of these systems.

ACKNOWLEDGMENTS

K.D.B. wishes to thank Dr. John Rose for many helpful discussions. This research was supported by Grant No. CHE-9414258 from the National Science Foundation.

[1] P. J. Robinson and K. A. Holbrook, *Unimolecular Reactions* (Wiley-Interscience, London, 1972).
[2] R. G. Gilbert and S. C. Smith, *Theory of Unimolecular and Recombination Reactions* (Blackwell Scientific, Oxford, 1990).
[3] F. H. Stillinger and T. A. Weber, Phys. Rev. A **25**, 978 (1982).
[4] F. G. Amar and R. S. Berry, J. Chem. Phys. **85**, 5943 (1986).
[5] I. R. McDonald, J. Chem. Soc. Faraday Discuss. **43**, 40 (1967).
[6] A. M. Ferrenberg and R. H. Swendsen, Phys. Rev. Lett. **63**, 1195 (1989).
[7] P. Labastie and R. L. Whetten, Phys. Rev. Lett. **65**, 1567 (1990).
[8] M. Vieth, A. Kolinski, and J. Skolnick, J. Chem. Phys. **102**, 6189 (1995).
[9] S. F. Chekmarev and I. H. Umirzakov, Z. Phys. D **26**, 373 (1993).
[10] J. P. K. Doye and D. J. Wales, J. Chem. Phys. **102**, 9659 (1995).
[11] B. Vekhter, K. D. Ball, J. Rose, and R. S. Berry, J. Chem. Phys. **106**, 4644 (1997).
[12] O. M. Becker and M. Karplus, J. Chem. Phys. **106**, 1495 (1997).
[13] J. P. Rose and R. S. Berry, J. Chem. Phys. **98**, 3246 (1993).
[14] J. N. Murrell and K. J. Laidler, J. Chem. Soc., Faraday Trans. **64**, 371 (1968).
[15] D. J. Wales and R. S. Berry, J. Chem. Soc., Faraday Trans. **88**, 543 (1992).
[16] N. Shida, J. E. Almlöf, and P. F. Barbara, Theor. Chim. Acta **76**, 7 (1989).
[17] N. Shida, Suuri Kagaku (Mathematical Physics, in Japanese) **396**, 50 (1996).
[18] J. P. Rose and R. S. Berry, J. Chem. Phys. **96**, 517 (1992).
[19] M. P. Tosi and F. G. Fumi, J. Phys. Chem. Solids **25**, 45 (1964).
[20] See Ref. 13 and references therein.
[21] W. H. Press, B. P. Flannery, S. A. Teukolsky, and W. T. Vetterling, *Numerical Recipes in Fortran*, 2nd. ed. (Cambridge University Press, Cambridge, 1992).
[22] Eigenvector-following and steepest-descent methods were performed with the OPTIM program provided by David Wales; D. J. Wales, J. Chem. Phys. **101**, 3750 (1994); D. J. Wales and T. R. Walsh, J. Chem. Phys. **105**, 6957 (1996).
[23] D. J. Wales, J. Chem. Soc., Faraday Trans. **88**, 653 (1992); **89**, 1305 (1993).
[24] M. Page and J. W. McIver, J. Chem. Phys. **88**, 922 (1988).
[25] J. E. Lennard-Jones, Proc. R. Soc. London, Ser. A **106**, 463 (1924).
[26] N. Bernardes, Phys. Rev. **112**, 1533 (1958).
[27] C. J. Tsai and K. D. Jordan, J. Phys. Chem. **97**, 11227 (1993).
[28] K. D. Ball, R. S. Berry, R. E. Kunz, F. Li, A. Proykova, and D. J. Wales, Science **271**, 963 (1996).
[29] R. E. Kunz and R. S. Berry, J. Chem. Phys. **103**, 1904 (1995).
[30] R. S. Berry and R. E. Kunz, Phys. Rev. Lett. **74**, 3951 (1995).
[31] R. E. Kunz, R. S. Berry, and T. Astakhova, Surf. Rev. Lett. **3**, 307 (1996).
[32] J. P. K. Doye and D. Wales, J. Chem. Phys. **105**, 8428 (1996).
[33] T. A. Witten, private communication.
[34] P. C. Haarhoff, Mol. Phys. **7**, 101 (1963).
[35] A. D. Isaacson, D. G. Truhlar, K. Scanlon, and J. Overend, J. Chem. Phys. **75**, 3017 (1981).
[36] A. Roitberg, R. B. Gerber, R. Elber, and M. A. Ratner, Science **268**, 1319 (1995).
[37] A. E. Roitberg, R. B. Gerber, and M. A. Ratner, J. Phys. Chem. B **101**, 1700 (1997).
[38] S. M. Kast, K. Nicklas, H-J Bär, and J. Brickmann, J. Chem. Phys. **100**, 566 (1994); S. M. Kast and J. Brickmann, J. Chem. Phys. **104**, 3732 (1996).